Inflammation, Vol. 47, No. 2, April 2024 (© 2024)
https://doi.org/10.1007/s10753-023-01926-y

RESEARCH

SLAMF7 Promotes Foam Cell Formation of Macrophage by Suppressing NR4A1 Expression During Carotid Atherosclerosis

Fengjiao Yuan[1,2,3] , Jianmei Wei[1] , Yan Cheng[1] , Feifei Wang[1] , Mingliang Gu[1] , Yanhui Li[4] , Xin Zhao[5] , Hao Sun[5] , Ru Ban[5] , Jing Zhou[6,7] and Zhangyong Xia[2,5,7]

Received 2 August 2023; accepted 20 October 2023

Abstract—Macrophage-derived lipid-laden foam cells from the subendothelium play a crucial role in the initiation and progression of atherosclerosis. However, the molecule mechanism that regulates the formation of foam cells is not completely understood. Here, we found that SLAMF7 was upregulated in mice bone marrow–derived macrophages and RAW264.7 cells stimulated with oxidized low-density lipoprotein (ox-LDL). SLAMF7 promoted ox-LDL-mediated macrophage lipid accumulation and M1-type polarization. SLAMF7 deficiency reduced serum lipid levels and improved the lesions area of carotid plaque and aortic arch in high-fat diet-fed ApoE$^{-/-}$ mice. In response to ox-LDL, SLAMF7 downregulated NR4A1 and upregulated RUNX3 through transcriptome sequencing analysis. Overexpression NR4A1 reversed SLAMF7-induced lipid uptake and M1 polarization via inhibiting RUNX3 expression. Furthermore, RUNX3 enhanced foam cell formation and M1-type polarization. Taken together, the study suggested that SLAMF7 play contributing roles in the pro-atherogenic effects by regulating NR4A1-RUNX3.

KEY WORDS: Carotid atherosclerosis; SLAMF7; foam cell formation; NR4A1; macrophage.

Fengjiao Yuan and Jianmei Wei contributed equally to this work.

[1]Joint Laboratory for Translational Medicine Research, Liaocheng People's Hospital, Liaocheng, Shandong 252000, People's Republic of China
[2]Department of Neurology, Liaocheng People's Hospital, Shandong University, Jinan, Shandong 250012, People's Republic of China
[3]Medical Integration and Practice Center, Shandong University, Jinan, Shandong 250012, People's Republic of China
[4]Department of Rehabilitation Medicine, Liaocheng Chinese Medicine Hospital, Liaocheng, Shandong 252000, People's Republic of China
[5]Department of Neurology, Liaocheng People's Hospital and Liaocheng Hospital Affiliated to Shandong First Medical University, Liaocheng, Shandong 252000, People's Republic of China
[6]Department of Neurology, The First Affiliated Hospital of Shandong First Medical University & Shandong Provincial Qianfoshan Hospital, Jinan, Shandong 250014, People's Republic of China
[7]To whom correspondence should be addressed at Department of Neurology, Liaocheng People's Hospital, Shandong University, Jinan, Shandong, 250012, People's Republic of China. Email: xiazhangyong2013@163.com and Department of Neurology, The First Affiliated Hospital of Shandong First Medical University & Shandong Provincial Qianfoshan Hospital, Jinan, Shandong, 250014, People's Republic of China. Email: zhoujingqy@126.com

INTRODUCTION

Carotid atherosclerosis (CAS) is a high-risk factor for ischemic strokes and a main cause of death and disability worldwide [1, 2]. The formation and development of atherosclerotic lesions are a chronic process characterized by the deposition of excessive lipid in the arterial intima [3, 4]. The current studies suggest multiple modifications of low-density lipoprotein (LDL) occurring in the blood or vessel wall, such as desialylation, lipid peroxidation, and the ability to aggregate, rather than native LDL, are the major source of lipids that accumulate in the atherosclerotic plaques [5]. Although the desialylation modification is likely the early and the most important modification, oxidized low-density lipoprotein (ox-LDL) modification is the most widely studied. Ox-LDL can stimulate inflammatory activation of macrophages, vascular smooth muscle cells, and other cells in the vicinity. In addition, LDL can be oxidized by malondialdehyde, copper, phosphatidylserine, and phosphorylcholine [6]. Accumulating evidence shows that macrophages play a critical role in all stages of atherosclerosis, from the lesion initiation, expansion, and rupture of the lesion [7]. Macrophages take up excessive ox-LDL and become engorged with lipids resulting in foam cell formation [8]. When these lipid-laden foam cells die and cannot be cleared from the subendothelium, they contribute to necrotic core formation and lead to plaque rupture and thrombosis [9, 10]. Therefore, understanding the molecular mechanisms involved in macrophage-derived foam cell formation is crucial for developing novel targets to combat CAS.

The signaling lymphocyte activation molecular family 7 (SLAMF7) is expressed on different types of cells such as NK cells, $CD8^+$ T cells, B cells, activated dendritic cells, and macrophages, affecting immune cell differentiation and function [11, 12]. Abnormal expression of SLAMF7 is involved in the development of various diseases, such as myeloma [13, 14], autoimmune disease [15, 16], and virus infection [17]. Recently, studies have shown that SLAMF7 has a double immunomodulatory effect on macrophages. On the one hand, SLAMF7 regulates protective immune to infectious microbes by inhibiting inflammatory responses and promoting M2 polarization of macrophages [18, 19]. On the other hand, SLAMF7 drives a strong wave of inflammatory cytokine expression, resulting in aberrant macrophage activation and pathological inflammation, such as Crohn's disease, rheumatoid arthritis, and severe COVID-19 disease [20].

We previously performed whole genome DNA methylation profiling, transcriptome sequencing analysis, and higher order pathological phenotypic analysis of carotid plaque from CAS patients. We revealed that SLAMF7 expression was upregulated on macrophage of carotid plaque, particularly in unstable plaque, and SLAMF7 deletion suppressed macrophage secretion of proinflammatory cytokines [21]. Macrophage-derived foam cell formation is the initial stage of atherosclerosis, and lipid-laden macrophage accumulation is also considered the symbol of unstable plaque [22]. However, the effect and mechanism of SLAMF7 on macrophage-derived foam cell formation are still unclear.

In this study, we found that ox-LDL induced increased expression of SLAMF7 in RAW264.7 cells and bone marrow–derived macrophages (BMDMs). SLAMF7 promoted ox-LDL-induced foam cell formation and M1 polarization in RAW264.7 cells. Meanwhile, deletion of SLAMF7 ameliorated carotid atherosclerosis in mice. Mechanistically, we demonstrated that SLAMF7 enhanced foam cell formation by inhibiting NR4A1 expression. When NR4A1 was inhibited, RUNX3 was upregulated in RAW264.7 cells, thereby promoting atherosclerosis.

MATERIALS AND METHODS

Reagents

Oxidized low-density lipoprotein (ox-LDL) was purchased from Yiyuan Biotechnologies (Guangzhou, China) [23, 24]. For preparation of ox-LDL, human LDL was purified to homogeneity via ultracentrifugation (1.019–1.063 g/cc) and was oxidized using Cu_2SO_4 in PBS at 37 °C for 18 h. Oxidation was terminated by adding excess EDTA-Na_2. Each lot was analyzed on agarose gel electrophoresis for migration versus LDL. This lot of ox-LDL migrated 2.0-fold further than the native LDL. Mouse macrophage colony-stimulating factor (M-CSF) was purchased from Peprotech (NJ, USA). β-Actin (3700S) and FLAG (14793S) antibody were acquired from Cell Signaling Technology (MA, USA). NR4A1 antibody was obtained from Proteintech (25851–1-AP, IL, USA). RUNX3 antibody was acquired from Santa Cruz (sc-376591, CA, USA). FITC Rat IgG2b, κ isotype control antibody (400633) and FITC anti-mouse CD86 antibody were purchased from BioLegend (CA, USA). qPCR-related reagents were purchased from Vazyme

(Shanghai, China). Western blot–related reagents were purchased from Beyotime (Nanjing, China).

Cell Culture and Stably Transfected Cell Line Generation

The RAW264.7 mouse macrophage cell line was obtained from Cell Bank of Chinese Academy of Sciences and cultured in Dulbecco's Modified Eagle's Medium (DMEM, Gibco, USA) supplemented with 10% fetal bovine serum (FBS, Gibco, USA) at 37 °C under a 5% CO_2 atmosphere.

To generate mouse BMDMs, C57BL/6 J mice were euthanized, and bone marrows in femurs were flushed out using a 25-G needle filled with DMEM medium following by filtering through a 70-μm strainer. The obtained bone marrow cells were then incubated in red blood cell lysis buffer (Solarbio, Beijing, China) for 10 min and washed with DMEM medium to remove red blood cells. Cells were cultured in DMEM supplemented with 10% FBS and 20 ng/mL murine M-CSF for 6 days with the medium refreshed every 2–3 days.

RAW264.7 cells were infected with lentivirus encoding SLAMF7 (GeneChem, Shanghai, China), NR4A1, and RUNX3 (OBiO Technology, Shanghai, China) and subjected to puromycin and blasticidins S selection, respectively. The overexpression was confirmed by qPCR and Western blot analysis.

To make lipid-loaded cells, RAW264.7 and BMDMs were stimulated with ox-LDL (50 μg/mL) for 24 h.

RNA Isolation and Quantitative Real-Time Polymerase Chain Reaction (qPCR)

Total RNA was isolated from cells with RNA isolater and reverse-transcribed to cDNA using HiScript® III RT SuperMix for qPCR kit. qPCR was carried out using ChamQ SYBR qPCR Master Kit in an ABI QuantStudio Q5 analyzer (Applied Biosystems, Thermo Fisher, USA). The relative mRNA expression levels of indicated genes were determined using the $2^{-\Delta\Delta Ct}$ method. The primers were synthesized from Sangon Biotech (Shanghai, China) and listed in Supplementary Table 1.

Western Blot

Cells were harvested, and cell lysates were resolved by sodium dodecyl sulfate–polyacrylamide gel electrophoresis (SDS-PAGE), then transferred to a polyvinylidene difluoride membrane. After blocking with 5% nonfat dry milk (BD Biosciences, USA) in TBST, the membranes were incubated with primary and secondary antibody (ZSGB-BIO, Beijing, China). Western blots were developed using a Gel Doc Imaging System (ChemiDoc MP, Bio-Rad, USA), and the intensities of bands were compared using ImageJ software.

Oil Red O (ORO) Staining

ORO staining was performed according to manufacturer's instructions (Solarbio, Beijing, China). Briefly, RAW264.7 cells were gently rinsed twice with PBS and fixed with ORO fixative for 30 min. After discarding fixative and washed twice with sterile water, the cells were pretreated with 60% isopropanol for 5 min and stained with ORO solution for 10 min. The cells were observed by light microscopy (×400), and the percentages of ORO positive cells in 5 microscopic fields for each independent experiment were counted and calculated.

Total Cholesterol Assay

The concentrations of total cholesterol in cells were measured using a total cholesterol assay kit (E1015, Applygen Technologies, Beijing, China). Briefly, after washed twice with PBS, RAW264.7 cells were added to 0.1 mL lysate and shaken for 10 min. The mixture was centrifuged at 2000 g for 5 min, and the supernatant was taken for enzymatic determination and BCA protein quantification. Cholesterol content was corrected with protein concentration per milligrams.

Flow Cytometry

RAW264.7 cells were collected and washed twice with cold PBS and then incubated with FITC-CD86 or isotype control antibody at 4 °C for 30 min. The cells were then analyzed and quantified using flow cytometry (CytoFLEX SRT, Beckman Coulter, USA).

Mouse Model and Atherosclerosis Assessment

Seven-week-old $ApoE^{-/-}$ mice were obtained from the Beijing Vital River Laboratory Animal Technology. The mice were randomly divided into four experimental groups (five mice per group). The Blank group was only fed a high-fat diet (HFD) for 13 weeks. The Control group, Negative control group (shNC), and SLAMF7

knockdown group (shSLAMF7) were fed HFD for 5 weeks, then injected with 150 µL PBS, 10^{11}vg control adeno-associated virus serotype type 9 (AAV9) vector carrying GFP, and AAV9-SLAMF7-short hairpin RNA (shRNA) (GeneChem, Shanghai, China) diluted in 150 µL PBS, respectively, via tail vein. Supplementing a HFD feeding for 1 more week, these three groups were carried on carotid ligation surgery as previously reported [25, 26]. HFD was continued for another 7 weeks. Finally, these mice were taken blood from heart and collected aortic arch and carotids. Aortic arch and carotids were fixed with 10% formalin and embedded with OCT or paraffin, respectively. They were stained with hematoxylin and eosin (H&E), ORO, Masson or Sirius Red staining for the evaluation of lesion area, lipid content, and collagen according to manufacturer's instructions (Solarbio, Beijing, China). The quantification of staining was measured by Image-Pro plus software (Media Cybernetics, MD, USA).

This study was performed in line with the principles of the Declaration of Helsinki. Animal experiment was conducted according to the Institutional Animal Care and Use Committee of the Model Animal Research Center. Approval was granted by the Ethics Committee of Liaocheng People's Hospital.

Serum Lipid Analysis

The serum total cholesterol (TC), triglyceride (TG), low-density lipoprotein cholesterol (LDL-C), and high-density lipoprotein cholesterol (HDL-C) levels were measured using biochemical kits (Biosino Bio-Technology and Science, Beijing, China) and Mindray BS-420 automatic biochemical analyzer.

RNA Sequencing

After isolation of total RNA, RNA integrity was evaluated using the Agilent Fragment Analyzer 5400 system. RNA libraries were prepared with the NEBNext® Ultra™ RNA Library Prep Kit for Illumina (New England Biolabs, MA, USA) described by the manufacturer. Samples were sequenced on Illumina NovaSeq 6000 instrument (Illumina, CA, USA). Raw reads were assessed for quality issues with FastQC [27] to ensure library generation and sequencing were suitable for further analysis. featureCounts v1.5.0-p3 [28] was used to count the reads numbers mapped to each gene. And then, FPKM of each gene was calculated based on the length of the gene and reads count mapped to this gene. Differentially expressed genes were identified with DESeq2 [29]. The resulting *P*-values were adjusted using the Benjamini-Hochberg's approach [30] to control the false discovery rate. The above experiments were completed with the assistance of Novogene (Beijing, China).

Statistical Analysis

Data were analyzed using GraphPad Prism 9.0 software. Two-sided Student's *t* test and one- or two-way ANOVA test were used to compare difference between groups. Data were displayed as the mean ± SD. A 95% confidence interval was considered significant and was defined as $P < 0.05$. $^{*}P < 0.05$, $^{**}P < 0.01$, $^{***}P < 0.001$.

RESULTS

Ox-LDL Induces SLAMF7 Expression in Macrophages

We have found that SLAMF7 is highly expressed in carotid plaque, especially in macrophages of unstable plaque [21]. However, its specific mechanism is still unclear. Foam cell formation, induced by uptaking of ox-LDL by macrophages in atherosclerotic plaques, is an important factor in the early onset of AS [31]. We cultured RAW264.7 cells and BMDMs with ox-LDL (50 µg/mL) for 24 h and found ox-LDL promoted the expression of SLAMF7 in macrophage (Fig. 1a, b).

SLAMF7 Promotes Ox-LDL-Induced Foam Cell Formation of Macrophages

We further investigated whether SLAMF7 could regulate foam cell formation in ox-LDL-activated macrophages via overexpressing SLAMF7 (Fig. 2a and Supplementary Fig. S1). ORO staining showed that compared with control cells, SLAMF7 overexpression significantly increased the lipid droplets area in RAW264.7 cells (Fig. 2b). In addition, SLAMF7 heightened total cholesterol levels in RAW264.7 cells (Fig. 2c). Macrophage-derived foam cells can release different inflammatory cytokines to affect the stability of plaque, and the change of M1/M2 phenotype of macrophages is a key factor in the regulation of inflammation [32]. Thus, we further explored the effect of SLAMF7 on macrophage polarization. In ox-LDL-treated macrophages, SLAMF7

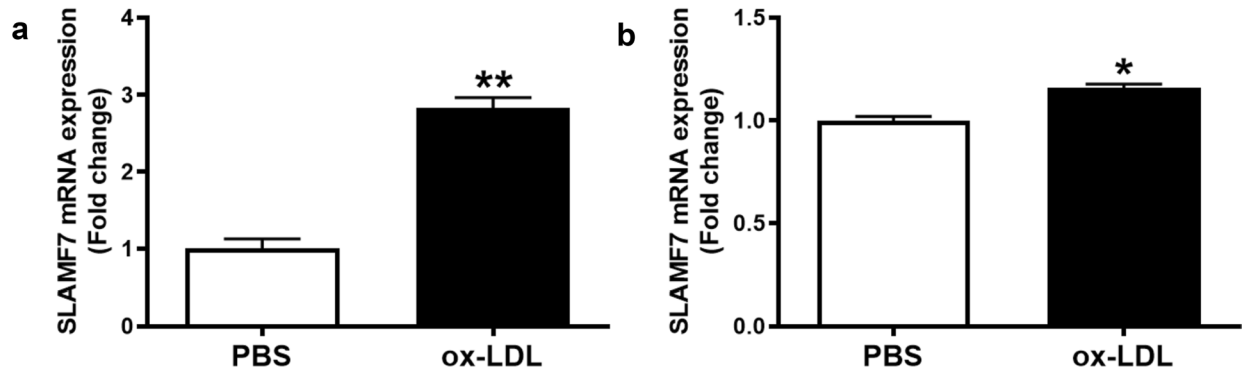

Fig. 1 ox-LDL-induced SLAMF7 expression in macrophages. **A** RAW264.7 or **B** BMDMs were stimulated by PBS or ox-LDL for 24 h, respectively. $*P<0.05$, $**P<0.01$.

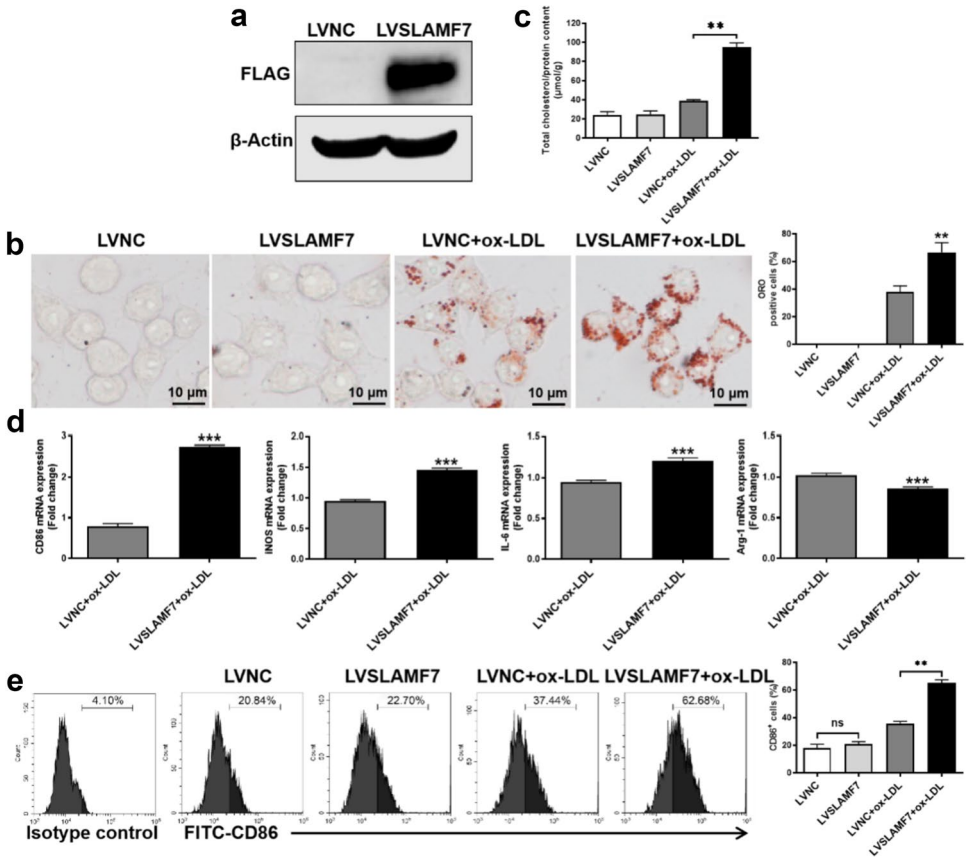

Fig. 2 SLAMF7 promoted ox-LDL-induced foam cell formation of macrophages. RAW264.7 cells were transfected with control or SLAMF7 lentiviruses and incubated with ox-LDL (50 μg/mL) for another 24 h. **A** Western blot analysis for SLAMF7 overexpression using FLAG antibody. **B** The lipid accumulation was measured by ORO staining in SLAMF7 overexpression RAW264.7 cells and control cells, respectively. The graph shows the proportion of ORO-positive cells. The scale: 10 μm. **C** Quantitative results of total cholesterol. **D** qPCR analysis for CD86, iNOS, IL-6, and Arg-1 expression. **E** Representative images and quantitative results of CD86 expression by flow cytometry. $**P<0.01$, $***P<0.001$.

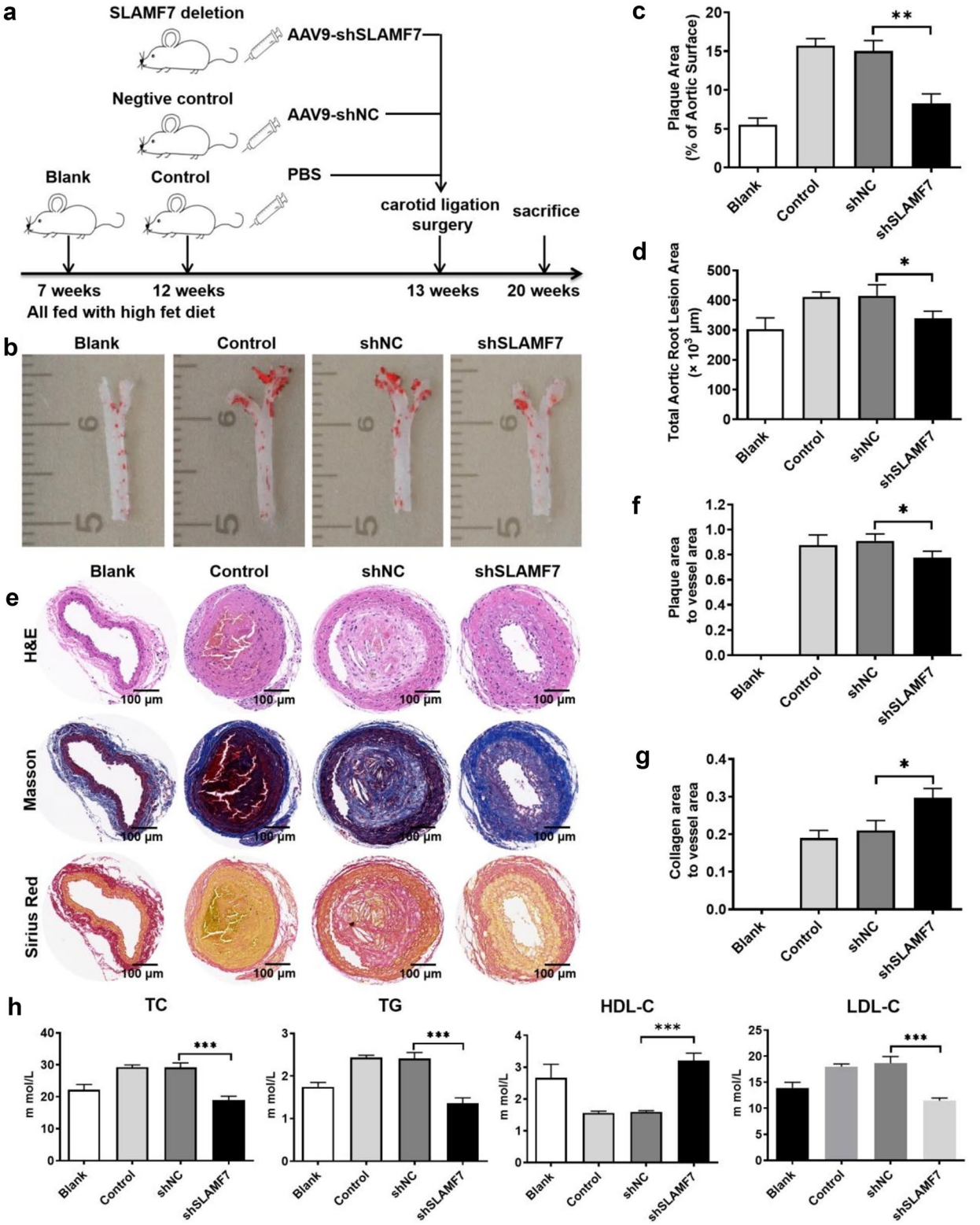
a
SLAMF7 deletion
AAV9-shSLAMF7
Negtive control
AAV9-shNC
PBS
Blank
Control
carotid ligation surgery
sacrifice
7 weeks
12 weeks
13 weeks
20 weeks
All fed with high fet diet
b
Blank
Control
shNC
shSLAMF7
c
Plaque Area (% of Aortic Surface)
d
Total Aortic Root Lesion Area (× 10³ μm)
e
H&E
Masson
Sirius Red
100 μm
f
Plaque area to vessel area
g
Collagen area to vessel area
h
TC
TG
HDL-C
LDL-C
m mol/L

◂**Fig. 3** Deletion of SLAMF7 alleviated the development of carotid atherosclerosis in mice. **A** Establishment of a mouse model with carotid atherosclerosis, adenovirus-associated virus was used to knock out SLAMF7. **B** Representative Oil Red O staining (red) in aortic arches of each group mouse. **C** Quantification of plaque area in aortas of mouse of each group as a percentage of total aorta area ($n=5$ per group). **D** Quantification of aortic root lesion area in each group mouse ($n=5$ per group). **E** H&E staining, Masson staining, and Sirius Red staining of carotid plaque in each group mouse. Scale bar: 100 μm. **F** Quantification of carotid plaque area to total vessel area. **G** Quantification of collagen area to total vessel area in carotid plaque. **H** Quantification of TC, TG, LDL-C, and HDL-C in serum of each group mouse. $^{*}P<0.05$, $^{**}P<0.01$, $^{***}P<0.001$.

overexpression upregulated the expression of iNOS, CD86, and IL-6 mRNA and downregulated the expression of Arg-1 mRNA (Fig. 2d). Flow cytometry results also showed that SLAMF7 promoted CD86 expression (Fig. 2e). These results demonstrated that SLAMF7 enhanced ox-LDL-induced foam cell formation and M1 polarization of macrophages.

Deletion of SLAMF7 Alleviates the Development of Carotid Atherosclerosis in Mice

To explore the role in carotid atherosclerosis of SLAMF7 *in vivo*, ApoE$^{-/-}$ mice underwent right-sided tandem stenosis carotid surgery 6 weeks after commencing HFD [33]. In the 5th week, AAV9-loaded SLAMF7 shRNA was injected with tail vein (Fig. 3a). GFP fluorescence intensity was observed in carotid artery to monitor the infection efficiency 2 weeks after injection (Supplementary Fig. S2). SLAMF7 deletion significantly decreased the lesion area in the *en face* ORO staining of aortic arch (Fig. 3b, c). We also observed the suppression in the atherosclerotic lesion area in the aortic roots of SLAMF7 deficient mice (Fig. 3d). Moreover, H&E, Masson, and Sirius Red staining revealed that deletion of SLAMF7 reduced carotid plaque burden with less necrotic core and more collagen (Fig. 3e–g). Meanwhile, the deficiency of SLAMF7 declined the levels of TC, TG, and LDL-C, but increased HDL-C in mouse serum (Fig. 3h). Together, these results indicated that SLAMF7 promoted the formation of carotid plaques in mice.

SLAMF7 Promotes Foam Cell Formation by Inhibiting NR4A1 Expression

In order to investigate the molecular mechanism of SLAMF7 in carotid atherosclerosis, we undertook transcriptome assay using RNA sequencing in SLAMF7 overexpression cells treated with ox-LDL. Multiple genes related to carotid atherosclerosis were identified by differential gene expression analysis, such as RGS1, TRIB1, MMP9, NR4A1, and RUNX3 (Fig. 4a, Supplementary Fig. S3, and Table S2). NR4A1 deficiency polarizes macrophages towards an inflammatory phenotype and enhances atherosclerosis [34–36]. We further confirmed that ox-LDL downregulated NR4A1 and upregulated RUXN3 expression and SLAMF7 amplified the effect through qPCR and Western blot analysis (Fig. 4b, c and Supplementary Fig. S4). Interestingly, in the absence of ox-LDL, overexpression of SLAMF7 alone had no effect on NR4A1 and RUNX3 expression compared with the vector group (Supplementary Fig. S4), which might explain why SLAMF7 overexpression alone without ox-LDL did not affect CD86 expression (Fig. 2). Wu *et al.* also found that without LPS, the mRNA levels of *Tnf*, *Il1b*, and *Il6* did not change in RAW264.7 cells stably expressing SLAMF7 versus control vector cells [18].

We next explored whether the overexpression of SLAMF7 promoted foam cell formation through inhibiting NR4A1 expression. To test this, lentiviruses overexpressing SLAMF7 and NR4A1 were co-transfected with RAW264.7 cells (Fig. 4d). ORO staining showed that compared with SLAMF7 overexpressing group, intracellular lipid droplet area was significantly reduced in SLAMF7 + NR4A1 overexpressing group (Fig. 4e). The concentration of total cholesterol also decreased in SLAMF7 and NR4A1 co-overexpression cells (Fig. 4f). Furthermore, NR4A1 inhibited SLAMF7-induced the expression of CD86 in response to ox-LDL (Fig. 4g). The above results illustrated that NR4A1 could reverse SLAMF7-induced macrophage foam cell formation and M1-type polarization.

SLAMF7 Promotes Foam Cell Formation by Regulating NR4A1-RUNX3

Previously reported that NR4A1 regulates the development and frequency of CD8^{+} T cells through direct transcriptional control of RUNX3 [37]; interestingly, we found SLAMF7 promoted RUNX3 expression, although inhibited NR4A1 according to the transcriptome sequencing assay (Fig. 3a). Likewise, NR4A1 reduced RUNX3 expression induced by SLAMF7 (Fig. 5a, b).

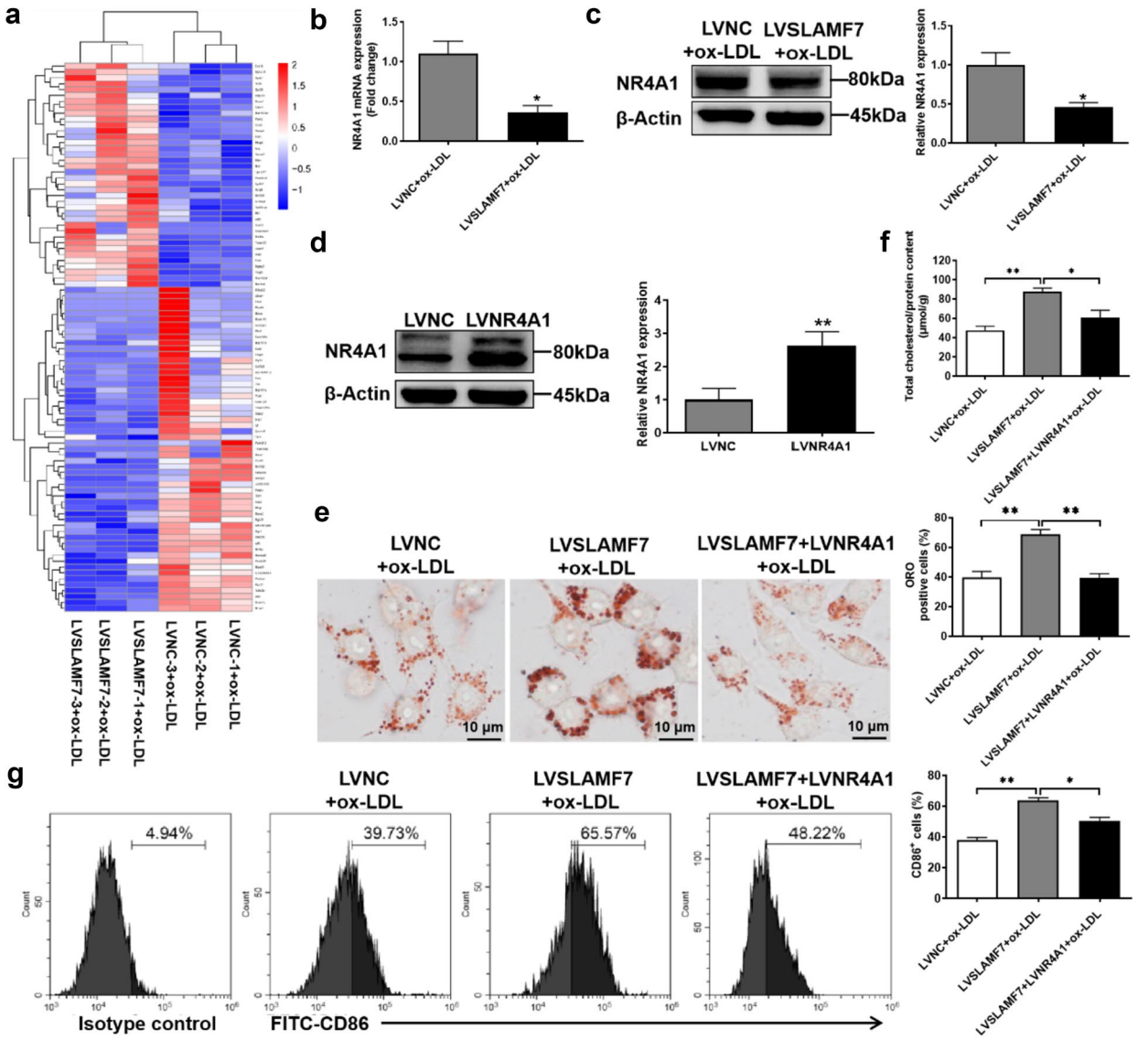

Fig. 4 SLAMF7 promoted carotid atherosclerosis by inhibiting NR4A1 expression. RAW264.7 cells were transfected with control or SLAMF7 lentiviruses and treated with ox-LDL (50 μg/mL) for another 24 h. **A** Differentially expressed gene heatmap of RAW264.7 cells (upregulated and downregulated genes) through transcriptome sequencing analysis. **B** qPCR analysis for NR4A1 expression. **C** Western blot and quantitative analysis for NR4A1 expression. **D–G** RAW264.7 cells were co-transfected with SLAMF7 and NR4A1 lentiviruses and incubated with ox-LDL (50 μg/mL) for another 24 h. **D** Western blot and quantitative analysis for NR4A1 expression after transfected with control or NR4A1 lentiviruses. **E** The lipid accumulation was measured by ORO staining. The graph shows the proportion of ORO-positive cells. The scale: 10 μm. **F** Quantitative results of total cholesterol. **G** Representative images and quantitative results of $CD86^+$ expression by flow cytometry. $^*P<0.05$, $^{**}P<0.01$.

Overexpression of RUNX3 increased foam cell formation and M1-type polarization (Fig. 5c–e). Together, the results suggested that SLAMF7 play contributing roles in the pro-atherogenic effects by regulating NR4A1-RUNX3.

DISCUSSION

Carotid atherosclerosis is an important pathological basis for the occurrence of ischemic stroke [38]. Accumulation of lipid-laden foam cells in the arterial wall

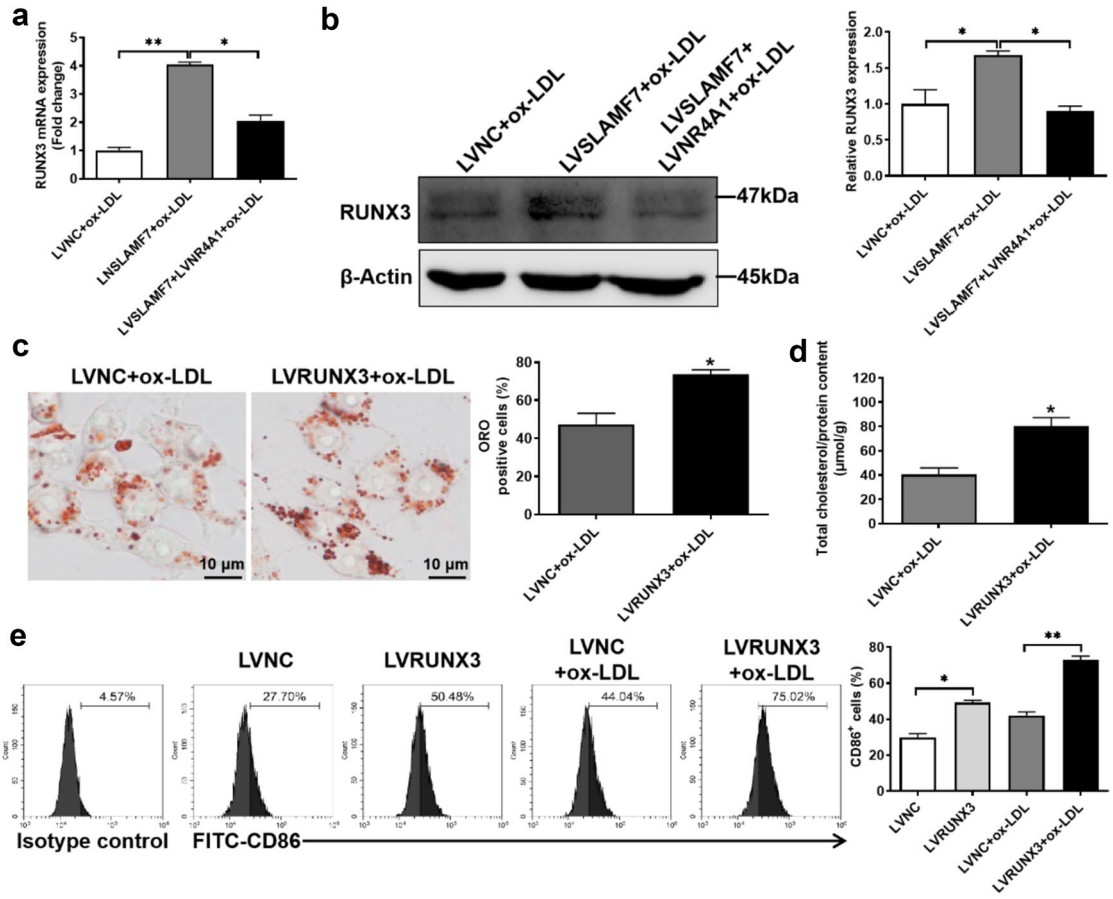

Fig. 5 SLAMF7 promotes foam cell formation by regulating NR4A1-RUNX3. RAW264.7 cells were co-transfected with SLAMF7 and NR4A1 lentiviruses and incubated with ox-LDL (50 μg/mL) for another 24 h. **A** qPCR analysis for RUNX3 expression. **B** Western blot and quantitative analysis for RUNX3 expression. **C**–**E** RAW264.7 cells were transfected with RUNX3 lentiviruses and treated with ox-LDL (50 μg/mL) for another 24 h. **C** The lipid accumulation was measured by ORO staining. The graph shows the proportion of ORO-positive cells. The scale: 10 μm. **D** Quantitative results of total cholesterol. **E** Representative images and quantitative results of $CD86^+$ expression by flow cytometry. $^*P < 0.05$, $^{**}P < 0.01$.

plays a central role in atherosclerotic lesion development, plaque progression, and late-stage complications of atherosclerosis [39, 40]. Therefore, a better cognition of the mechanism leading to foam cell formation may discover the new therapeutic targets for atherosclerosis. Nonetheless, it is remain poorly understood. Here, we reported that SLAMF7 influenced the occurrence and development of CAS by inducing macrophage-derived foam cell formation.

As an important driver in atherosclerosis, foam cells are regulated by a complex network of interacting genes and proteins [41]. The accumulation of ox-LDL in macrophages is the initial step in the foam cell formation [42, 43]. In our study, we found that ox-LDL stimulated the expression of SLAMF7 in macrophages. The upregulated SLAMF7 promoted ox-LDL-inducing foam cell formation, which was shown in the increase of lipid droplet area and total cholesterol content in SLAMF7 overexpression cells. Foam cell formation is related to the significant changes of many kinds of lipids [44]. In SLAMF7 deficiency $ApoE^{-/-}$ mice, the levels of TC, TG, and LDL-C were lessened, but HDL-C was risen. We also observed the reduction of plaque area, necrosis core, and lipid deposition in SLAMF7 deficiency mice by histopathological staining. All these indicated that SLAMF7 promoted atherogenesis. It has been reported that atherosclerosis is an immune system–mediated, chronic inflammatory disease [45]. M1 inflammatory

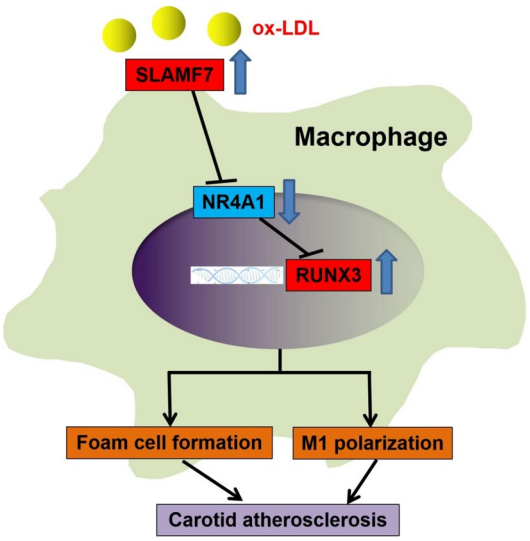

Fig. 6 Schematic illustration of SLAMF7-NR4A1-RUNX3 pathway in foam cell formation of macrophage during carotid atherosclerosis

macrophages predominate in the progression of atherosclerosis plaque, and M2 anti-inflammatory macrophages play a leading role in the regression of plaque [46]. In our study, we found that SLAMF7 induced the expression of iNOS, CD86, IL-6, and suppressed the expression of Arg-1 in ox-LDL stimulated macrophages. SLAMF7 regulates immune balance in monocytes/macrophages. Studies have shown that IFN-γ can regulate SLAMF7 expression, thereby driving an inflammatory signaling cascade in macrophages of inflammatory synovial tissue [20]. In the initial stage of viral or bacterial infection, the elevated SLAMF7 promotes inflammation, while in the later stage, the sustained high expression of SLAMF7 alleviates inflammation by promoting macrophage M2 polarization [19]. Thus, SLAMF7 may also affect atherosclerosis by modulating macrophage M1-type polarization.

We next employed transcriptome assay using RNA sequencing to reveal that NR4A1 was inhibited in macrophages overexpressed with SLAMF7. In response to ox-LDL, overexpression of NR4A1 could reverse SLAMF7-inducing foam cell formation. In line with our observation, previous findings reveal that NR4A1 alleviates atherosclerosis by decreasing macrophage NLRP3 inflammasome-mediated inflammation [47]. NR4A1 deletion in bone marrow or marginal zone B cells accelerates atherosclerosis [35, 48]. In addition, NR4A1 deficiency polarizes macrophages towards an inflammatory phenotype, leading to aggravation of atherosclerosis [34, 36]. We also found that overexpression of NR4A1 downregulated SLAMF7-induced macrophage CD86 expression. All of these findings suggested that SLAMF7 may promote macrophage foam formation by downregulating NR4A1.

Interestingly, we also found that SLAMF7 promoted RUNX3 expression; however, NR4A1 blocked this effect. Moreover, RUNX3 could increase lipid droplet area and M1 polarization in ox-LDL-stimulated macrophages, which leading to foam cell formation. Previous findings reveal that RUNX3 may play a role in inflammation and metabolism of atherosclerosis by regulating Th17 and monocytes [49–52].

In summary, we reported that SLAMF7 had a pro-atherogenic role in facilitating the foam cell formation by regulating NR4A1-RUNX3 (Fig. 6). This finding pointed to the potential of SLAMF7 as a therapeutic target for atherosclerosis.

SUPPLEMENTARY INFORMATION

The online version contains supplementary material available at https://doi.org/10.1007/s10753-023-01926-y.

AUTHOR CONTRIBUTION

Fengjiao Yuan and Jianmei Wei designed study, performed research, analyzed data, and wrote the paper. Yan Cheng and Feifei Wang performed research. Mingliang Gu and Yanhui Li guided experimental techniques. Xin Zhao, Hao Song, and Ru Ban interpreted pathology. Jing Zhou and Zhangyong Xia designed study, and revised the article. All authors read and approved the final manuscript.

FUNDING

This work was supported by the Natural Science Foundation of Shandong Province (ZR2020MH139) and Shandong Province Postdoctoral Innovation Project (2021151).

DATA AVAILABILITY

The data that support the findings of this study are available from the corresponding author upon reasonable request.

DECLARATIONS

Ethics Approval This study was performed in line with the principles of the Declaration of Helsinki. Animal

experiment was conducted according to the Institutional Animal Care and Use Committee of the Model Animal Research Center. Approval was granted by the Ethics Committee of Liaocheng People's Hospital.

Competing Interests The authors have no relevant financial or non-financial interests to disclose.

REFERENCES

1. Bonati L. H., O. Jansen, G. J. de Borst, M. M. Brown. 2022. Management of atherosclerotic extracranial carotid artery stenosis. *Lancet Neurology* 21 (3):273–283. https://doi.org/10.1016/S1474-4422(21)00359-8.
2. Tzoulaki I., R. Castagné, C. L. Boulangé, I. Karaman, E. Chekmeneva, E. Evangelou, T. M. D. Ebbels, M. R. Kaluarachchi, M. Chadeau-Hyam, D. Mosen, A. Dehghan, A. Moayyeri, D. L. S. Ferreira, X. Guo, J. I. Rotter, K. D. Taylor, M. Kavousi, P. S. de Vries, B. Lehne, M. Loh, A. Hofman, J. K. Nicholson, J. Chambers, C. Gieger, E. Holmes, R. Tracy, J. Kooner, P. Greenland, O. H. Franco, D. Herrington, J. C. Lindon, P. Elliott. 2019. Serum metabolic signatures of coronary and carotid atherosclerosis and subsequent cardiovascular disease. *European Heart Journal* 40 (34):2883–2896. https://doi.org/10.1093/eurheartj/ehz235.
3. Liu Z., H. Zhu, X. Dai, C. Wang, Y. Ding, P. Song, M. H. Zou. 2017. Macrophage liver kinase B1 inhibits foam cell formation and atherosclerosis. *Circulation Research* 121 (9):1047–1057. https://doi.org/10.1161/CIRCRESAHA.117.311546.
4. Libby P., J. E. Buring, L. Badimon, G. K. Hansson, J. Deanfield, M. S. Bittencourt, L. Tokgozoglu, E. F. Lewis. 2019. Atherosclerosis. *Nature Reviews Disease Primers* 5 (1):56. https://doi.org/10.1038/s41572-019-0106-z.
5. Summerhill V. I., A. V. Grechko, S. F. Yet, I. A. Sobenin, A. N. Orekhov. 2019. The atherogenic role of circulating modified lipids in atherosclerosis. *International Journal of Molecular Sciences* 20 (14). https://doi.org/10.3390/ijms20143561.
6. Hartley A., D. Haskard, R. Khamis. 2019. Oxidized LDL and anti-oxidized LDL antibodies in atherosclerosis - novel insights and future directions in diagnosis and therapy<sup/>. *Trends in Cardiovascular Medicine* 29 (1):22–26. https://doi.org/10.1016/j.tcm.2018.05.010.
7. Tabas I., K. E. Bornfeldt. 2020. Intracellular and intercellular aspects of macrophage immunometabolism in atherosclerosis. *Circulation Research* 126 (9):1209–1227. https://doi.org/10.1161/CIRCRESAHA.119.315939.
8. Back M., A. Yurdagul, Jr., I. Tabas, K. Oorni, P. T. Kovanen. 2019. Inflammation and its resolution in atherosclerosis: mediators and therapeutic opportunities. *Nature Reviews Cardiology* 16 (7):389–406. https://doi.org/10.1038/s41569-019-0169-2.
9. Libby P., G. Pasterkamp, F. Crea, I. K. Jang. 2019. Reassessing the mechanisms of acute coronary syndromes. *Circulation Research* 124 (1):150–160. https://doi.org/10.1161/CIRCRESAHA.118.311098.
10. Doddapattar P., R. Dev, M. Ghatge, R. B. Patel, M. Jain, N. Dhanesha, S. R. Lentz, A. K. Chauhan. 2022. Myeloid cell PKM2 deletion enhances efferocytosis and reduces atherosclerosis. *Circulation Research* 130 (9):1289–1305. https://doi.org/10.1161/CIRCRESAHA.121.320704.
11. Malaer J. D., A. M. Marrufo, P. A. Mathew. 2019. 2B4 (CD244, SLAMF4) and CS1 (CD319, SLAMF7) in systemic lupus erythematosus and cancer. *Clinical Immunology* 204:50–56. https://doi.org/10.1016/j.clim.2018.10.009.
12. Cannons J. L., S. G. Tangye, P. L. Schwartzberg. 2011. SLAM family receptors and SAP adaptors in immunity. *Annual Review of Immunology* 29:665–705. https://doi.org/10.1146/annurev-immunol-030409-101302.
13. Lonial S., M. Dimopoulos, A. Palumbo, D. White, S. Grosicki, I. Spicka, A. Walter-Croneck, P. Moreau, M. V. Mateos, H. Magen, A. Belch, D. Reece, M. Beksac, A. Spencer, H. Oakervee, R. Z. Orlowski, M. Taniwaki, C. Rollig, H. Einsele, K. L. Wu, A. Singhal, J. San-Miguel, M. Matsumoto, J. Katz, E. Bleickardt, V. Poulart, K. C. Anderson, P. Richardson, E.-. Investigators. 2015. Elotuzumab therapy for relapsed or refractory multiple myeloma. *The New England Journal of Medicine* 373 (7):621–631. https://doi.org/10.1056/NEJMoa1505654.
14. O'Neal J., J. K. Ritchey, M. L. Cooper, J. Niswonger, L. Sofia Gonzalez, E. Street, M. P. Rettig, S. W. Gladney, L. Gehrs, R. Abboud, J. L. Prior, G. J. Haas, R. G. Jayasinghe, L. Ding, A. Ghobadi, R. Vij, J. F. DiPersio. 2022. CS1 CAR-T targeting the distal domain of CS1 (SLAMF7) shows efficacy in high tumor burden myeloma model despite fratricide of CD8+CS1 expressing CAR-T cells. *Leukemia* 36 (6):1625–1634. https://doi.org/10.1038/s41375-022-01559-4.
15. O'Connell P., M. K. Blake, S. Godbehere, A. Amalfitano, Y. A. Aldhamen. 2022. SLAMF7 modulates B cells and adaptive immunity to regulate susceptibility to CNS autoimmunity. *Journal of Neuroinflammation* 19 (1):241. https://doi.org/10.1186/s12974-022-02594-9.
16. Comte D., M. P. Karampetsou, N. Yoshida, K. Kis-Toth, V. C. Kyttaris, G. C. Tsokos. 2017. Signaling lymphocytic activation molecule family member 7 engagement restores defective effector CD8+ T cell function in systemic lupus erythematosus. *Arthritis Rheumatology* 69 (5):1035–1044. https://doi.org/10.1002/art.40038.
17. O'Connell P., Y. Pepelyayeva, M. K. Blake, S. Hyslop, R. B. Crawford, M. D. Rizzo, C. Pereira-Hicks, S. Godbehere, L. Dale, P. Gulick, N. E. Kaminski, A. Amalfitano, Y. A. Aldhamen. 2019. SLAMF7 is a critical negative regulator of IFN-alpha-mediated CXCL10 production in chronic HIV infection. *The Journal of Immunology* 202 (1):228–238. https://doi.org/10.4049/jimmunol.1800847.
18. Wu Y., Q. Wang, M. Li, J. Lao, H. Tang, S. Ming, M. Wu, S. Gong, L. Li, L. Liu, X. Huang. 2023. SLAMF7 regulates the inflammatory response in macrophages during polymicrobial sepsis. *The Journal of Clinical Investigation* 133 (6). https://doi.org/10.1172/jci150224.
19. Zhu S., Y. Chen, J. Lao, C. Wu, X. Zhan, Y. Wu, Y. Shang, Z. Zou, J. Zhou, X. Ji, X. Huang, X. Shi, M. Wu. 2021. Signaling lymphocytic activation molecule family-7 alleviates corneal inflammation by promoting M2 polarization. *The Journal of Infectious Diseases* 223 (5):854–865. https://doi.org/10.1093/infdis/jiaa445.
20. Simmons D. P., H. N. Nguyen, E. Gomez-Rivas, Y. Jeong, A. H. Jonsson, A. F. Chen, J. K. Lange, G. S. Dyer, P. Blazar, B. E. Earp, J. S. Coblyn, E. M. Massarotti, J. A. Sparks, D. J. Todd, R. A. S. L. E. N. Accelerating Medicines Partnership, D. A. Rao, E. Y. Kim, M. B. Brenner. 2022. SLAMF7 engagement superactivates macrophages in acute and chronic inflammation. *Science Immunology* 7 (68):eabf2846. https://doi.org/10.1126/sciimmunol.abf2846.

21. Xia, Z.G.M., X. Jia, X. Wang, C. Wu, J. Guo, L. Zhang, Y. Du, and J. Wang. 2018. Integrated DNA methylation and gene expression analysis identifies SLAMF7 as a key regulator of atherosclerosis. *Aging* 10 (6): 1324–1337.
22. Wang C., W. Yang, X. Liang, W. Song, J. Lin, Y. Sun, X. Guan. 2020. MicroRNA-761 modulates foam cell formation and inflammation through autophagy in the progression of atherosclerosis. *Molecular and Cellular Biochemistry* 474 (1–2):135–146. https://doi.org/10.1007/s11010-020-03839-y.
23. Fang S., X. Wan, X. Zou, S. Sun, X. Hao, C. Liang, Z. Zhang, F. Zhang, B. Sun, H. Li, B. Yu. 2021. Arsenic trioxide induces macrophage autophagy and atheroprotection by regulating ROS-dependent TFEB nuclear translocation and AKT/mTOR pathway. *Cell Death & Disease* 12 (1):88. https://doi.org/10.1038/s41419-020-03357-1.
24. Fu X., X. Yu, J. Jiang, J. Yang, L. Chen, Z. Yang, C. Yu. 2022. Small molecule-assisted assembly of multifunctional ceria nanozymes for synergistic treatment of atherosclerosis. *Nature Communications* 13 (1):6528. https://doi.org/10.1038/s41467-022-34248-y.
25. Yang Z., Y. Huang, L. Zhu, K. Yang, K. Liang, J. Tan, B. Yu. 2021. SIRT6 promotes angiogenesis and hemorrhage of carotid plaque via regulating HIF-1alpha and reactive oxygen species. *Cell Death & Disease* 12 (1):77. https://doi.org/10.1038/s41419-020-03372-2.
26. Zhang K., J. Zheng, Y. Chen, J. Dong, Z. Li, Y. P. Chiang, M. He, Q. Huang, H. Tang, X. C. Jiang. 2021. Inducible phospholipid transfer protein deficiency ameliorates atherosclerosis. *Atherosclerosis* 324:9–17. https://doi.org/10.1016/j.atherosclerosis.2021.03.011.
27. Andrews S. 2010. FastQC: a quality control tool for high throughput sequence data. Babraham Bioinformatics, Babraham Institute, Cambridge, United Kingdom,
28. Liao Y., G. K. Smyth, W. Shi. 2014. featureCounts: an efficient general purpose program for assigning sequence reads to genomic features. *Bioinformatics (Oxford, England)* 30 (7):923–930. https://doi.org/10.1093/bioinformatics/btt656.
29. Love M. I., W. Huber, S. Anders. 2014. Moderated estimation of fold change and dispersion for RNA-seq data with DESeq2. *Genome Biology* 15 (12):550. https://doi.org/10.1186/s13059-014-0550-8.
30. Benjamini Y., Y. J. J. o. t. R. s. s. s. B. Hochberg. 1995. Controlling the false discovery rate: a practical and powerful approach to multiple testing. 57 (1):289–300.
31. Johnston JM A. A., Bauer RC, Hamby S, Suvarna SK, Baidžajevas K, Hegedus Z, Dear TN, Turner M; Cardiogenics Consortium; Wilson HL, Goodall AH, Rader DJ, Shoulders CC, Francis SE, Kiss-Toth E. 2019. Myeloid Tribbles 1 induces early atherosclerosis via enhanced foam cell expansion. *Science Advances* 5 (10):eaax9183.
32. Li H., Z. Cao, L. Wang, C. Liu, H. Lin, Y. Tang, P. Yao. 2022. Macrophage subsets and death are responsible for atherosclerotic plaque formation. *Front Immunology* 13:843712. https://doi.org/10.3389/fimmu.2022.843712.
33. Schwarz N., S. Fernando, Y. C. Chen, T. Salagaras, S. R. Rao, S. Liyanage, A. E. Williamson, D. Toledo-Flores, C. Dimasi, T. J. Sargeant, J. Manavis, E. Eddy, P. Kanellakis, P. L. Thompson, J. T. M. Tan, M. F. Snel, C. A. Bursill, S. J. Nicholls, K. Peter, P. J. Psaltis. 2023. Colchicine exerts anti-atherosclerotic and -plaque-stabilizing effects targeting foam cell formation. *FASEB Journal* 37 (4):e22846. https://doi.org/10.1096/fj.202201469R.
34. Hanna R. N., I. Shaked, H. G. Hubbeling, J. A. Punt, R. Wu, E. Herrley, C. Zaugg, H. Pei, F. Geissmann, K. Ley, C. C. Hedrick. 2012. NR4A1 (Nur77) deletion polarizes macrophages toward an inflammatory phenotype and increases atherosclerosis. *Circulation Research* 110 (3):416–427. https://doi.org/10.1161/CIRCRESAHA.111.253377.
35. Hamers A. A., M. Vos, F. Rassam, G. Marinkovic, K. Kurakula, P. J. van Gorp, M. P. de Winther, M. J. Gijbels, V. de Waard, C. J. de Vries. 2012. Bone marrow-specific deficiency of nuclear receptor Nur77 enhances atherosclerosis. *Circulation Research* 110 (3):428–438. https://doi.org/10.1161/CIRCRESAHA.111.260760.
36. Koenis D. S., L. Medzikovic, P. B. van Loenen, M. van Weeghel, S. Huveneers, M. Vos, I. J. Evers-van Gogh, J. Van den Bossche, D. Speijer, Y. Kim, L. Wessels, N. Zelcer, W. Zwart, E. Kalkhoven, C. J. de Vries. 2018. Nuclear receptor Nur77 limits the macrophage inflammatory response through transcriptional reprogramming of mitochondrial metabolism. *Cell Reports* 24 (8):2127–2140 e2127. https://doi.org/10.1016/j.celrep.2018.07.065.
37. Nowyhed H. N., T. R. Huynh, A. Blatchley, R. Wu, G. D. Thomas, C. C. Hedrick. 2015. The nuclear receptor nr4a1 controls CD8 T cell development through transcriptional suppression of runx3. *Scientific Reports* 5:9059. https://doi.org/10.1038/srep09059.
38. Song P., Z. Fang, H. Wang, Y. Cai, K. Rahimi, Y. Zhu, F. G. R. Fowkes, F. J. I. Fowkes, I. Rudan. 2020. Global and regional prevalence, burden, and risk factors for carotid atherosclerosis: a systematic review, meta-analysis, and modelling study. *Lancet Global Health* 8 (5):e721-e729. https://doi.org/10.1016/S2214-109X(20)30117-0.
39. Lin H. P., B. Singla, W. Ahn, P. Ghoshal, M. Blahove, M. Cherian-Shaw, A. Chen, A. Haller, D. Y. Hui, K. Dong, J. Zhou, J. White, A. M. Stranahan, A. Jasztal, R. Lucas, B. K. Stansfield, D. Fulton, S. Chlopicki, G. Csanyi. 2022. Receptor-independent fluid-phase macropinocytosis promotes arterial foam cell formation and atherosclerosis. *Science Translational Medicine* 14 (663):eadd2376. https://doi.org/10.1126/scitranslmed.add2376.
40. Liu X., J. W. Guo, X. C. Lin, Y. H. Tuo, W. L. Peng, S. Y. He, Z. Q. Li, Y. C. Ye, J. Yu, F. R. Zhang, M. M. Ma, J. Y. Shang, X. F. Lv, A. D. Zhou, Y. Ouyang, C. Wang, R. P. Pang, J. X. Sun, J. S. Ou, J. G. Zhou, S. J. Liang. 2021. Macrophage NFATc3 prevents foam cell formation and atherosclerosis: evidence and mechanisms. *European Heart Journal* 42 (47):4847–4861. https://doi.org/10.1093/eurheartj/ehab660.
41. Wang D., Y. Yang, Y. Lei, N. T. Tzvetkov, X. Liu, A. W. K. Yeung, S. Xu, A. G. Atanasov. 2019. Targeting foam cell formation in atherosclerosis: therapeutic potential of natural products. *Pharmacological Reviews* 71 (4):596–670. https://doi.org/10.1124/pr.118.017178.
42. Wang B., X. Tang, L. Yao, Y. Wang, Z. Chen, M. Li, N. Wu, D. Wu, X. Dai, H. Jiang, D. Ai. 2022. Disruption of USP9X in macrophages promotes foam cell formation and atherosclerosis. *Journal of Clinical Investigation* 132 (10). https://doi.org/10.1172/JCI154217.
43. Pi S., L. Mao, J. Chen, H. Shi, Y. Liu, X. Guo, Y. Li, L. Zhou, H. He, C. Yu, J. Liu, Y. Dang, Y. Xia, Q. He, H. Jin, Y. Li, Y. Hu, Y. Miao, Z. Yue, B. Hu. 2021. The P2RY12 receptor promotes VSMC-derived foam cell formation by inhibiting autophagy in advanced atherosclerosis. *Autophagy* 17 (4):980–1000. https://doi.org/10.1080/15548627.2020.1741202.
44. Spann N. J., L. X. Garmire, J. G. McDonald, D. S. Myers, S. B. Milne, N. Shibata, D. Reichart, J. N. Fox, I. Shaked, D. Heudobler, C. R. Raetz, E. W. Wang, S. L. Kelly, M. C. Sullards, R. C. Murphy, A. H. Merrill, Jr., H. A. Brown, E. A. Dennis, A. C. Li, K. Ley, S. Tsimikas, E. Fahy, S. Subramaniam, O. Quehenberger, D. W. Russell, C. K. Glass. 2012. Regulated accumulation

of desmosterol integrates macrophage lipid metabolism and inflammatory responses. *Cell* 151 (1):138–152. https://doi.org/10.1016/j.cell.2012.06.054.

45. Engelen S. E., A. J. B. Robinson, Y. X. Zurke, C. Monaco. 2022. Therapeutic strategies targeting inflammation and immunity in atherosclerosis: how to proceed? *Nature Reviews Cardiology* 19 (8):522–542. https://doi.org/10.1038/s41569-021-00668-4.
46. Jinnouchi H., L. Guo, A. Sakamoto, S. Torii, Y. Sato, A. Cornelissen, S. Kuntz, K. H. Paek, R. Fernandez, D. Fuller, N. Gadhoke, D. Surve, M. Romero, F. D. Kolodgie, R. Virmani, A. V. Finn. 2020. Diversity of macrophage phenotypes and responses in atherosclerosis. *Cellular and Molecular Life Sciences* 77 (10):1919–1932. https://doi.org/10.1007/s00018-019-03371-3.
47. Ruosen Y., W. Zhang, P. Nie, K. Lan, X. Yang, A. Yin, Q. Xiao, Y. Shen, K. Xu, X. Wang, X. Pan, L. Shen, B. He. 2022. Nur77 deficiency exacerbates macrophage NLRP3 inflammasome-mediated inflammation and accelerates atherosclerosis. *Oxidative Medicine and Cellular Longevity* 2022:2017815. https://doi.org/10.1155/2022/2017815.
48. Nus M., G. Basatemur, M. Galan, L. Cros-Brunso, T. X. Zhao, L. Masters, J. Harrison, N. Figg, D. Tsiantoulas, F. Geissmann, C. J. Binder, A. P. Sage, Z. Mallat. 2020. NR4A1 deletion in marginal zone B cells exacerbates atherosclerosis in mice-brief report. *Arteriosclerosis, Thrombosis, and Vascular Biology* 40 (11):2598–2604. https://doi.org/10.1161/ATVBAHA.120.314607.
49. Bao M. H., H. Q. Luo, L. H. Chen, L. Tang, K. F. Ma, J. Xiang, L. P. Dong, J. Zeng, G. Y. Li, J. M. Li. 2016. Impact of high fat diet on long non-coding RNAs and messenger RNAs expression in the aortas of ApoE(-/-) mice. *Scientific Reports* 6:34161. https://doi.org/10.1038/srep34161.
50. Su Z., H. Lu, H. Jiang, H. Zhu, Z. Li, P. Zhang, P. Ni, H. Shen, W. Xu, H. Xu. 2015. IFN-gamma-producing Th17 cells bias by HMGB1-T-bet/RUNX3 axis might contribute to progression of coronary artery atherosclerosis. *Atherosclerosis* 243 (2):421–428. https://doi.org/10.1016/j.atherosclerosis.2015.09.037.
51. Shao Y., F. Saaoud, W. Cornwell, K. Xu, A. Kirchhoff, Y. Lu, X. Jiang, H. Wang, T. J. Rogers, X. Yang. 2022. Cigarette smoke and morphine promote treg plasticity to Th17 via enhancing trained immunity. *Cells* 11 (18). https://doi.org/10.3390/cells11182810.
52. Dybska E., J. K. Nowak, J. Walkowiak. 2023. Transcriptomic context of RUNX3 expression in monocytes: a cross-sectional analysis. *Biomedicines* 11 (6). https://doi.org/10.3390/biomedicines11061698.